Structural and transport properties of $CuSc_{1-x}Mg_xO_{2+y}$ delafossites

R. Kykyneshi, B. C. Nielsen, and J. Tate
Department of Physics, Oregon State University, Corvallis, Oregon 97331

J. Li and A. W. Sleight
Department of Chemistry, Oregon State University, Corvallis, Oregon 97331

(Received 17 May 2004; accepted 23 August 2004)

Transport and structural properties of Mg-doped and O-intercalated sintered powders and polycrystalline films of $CuSc_{1-x}Mg_xO_{2+y}$ are reported. Substitution of Mg for Sc systematically increases the *p*-type conductivity in $CuSc_{1-x}Mg_xO_2$ sintered powders, producing a maximum conductivity of 0.015 S/cm at $x \approx 0.06$. A similar level of conductivity is observed in transparent polycrystalline $CuSc_{1-x}Mg_xO_2$ films at the same doping level. Mg doping causes no significant increase in optical absorption at this level. Intercalation of oxygen into the delafossite structure leads to a much larger increase in *p*-type conductivity. In powders, the maximum conductivity is 0.5 S/cm at $y=0.23$ and $x=0.05$. In oxygen-intercalated films, the maximum conductivity was 25 S/cm, with the transparent films gradually darkening as oxygen is incorporated. Oxygen intercalation increases the *a*-axis lattice parameter of the delafossite structure in both films and powders, with a much smaller effect on the *c*-axis parameter. Two distinct phases with $y \approx 0$ and $y \approx 0.5$ are observed in x-ray diffraction of powders. In films intermediate values of *y* are observed, often in combination with a distinct $y=0$ phase. The absorption properties of the powder samples indicate introduction of defects into the 2H polymorph of $CuScO_2$ and $CuSc_{1-x}Mg_xO_2$ compared to the 3R polymorph. © *2004 American Institute of Physics*. [DOI: 10.1063/1.1806256]

I. INTRODUCTION

Oxides with the delafossite structure ($CuFeO_2$) have attracted interest as *p*-type transparent conductors. They are also of interest because they exhibit negative thermal expansion,[1] they are examples of frustrated magnetic systems,[2] and they are also potential thermoelectric materials.[3] Thin films are of particular interest, since it is in this form that applications are most likely to be realized, and there are reports of thin films of $CuScO_2$,[4,5] $CuAlO_2$,[6] $CuInO_2$,[7] and $CuGaO_2$.[8] However, investigation of electronic bulk properties is also important because control and measurement of some parameters, such as oxygen content, is easier in bulk than in films.[9–11]

Delafossites with $A=Cu^+$ in the AMO_2 structure are by far the most studied. These, and similar materials with $A=Ag^+$, are generally semiconductors,[12] and are usually transparent when stoichiometric. The *p*-type conductivity of the semiconducting delafossite derives from the introduction of holes into a predominantly Cu-3*d* valence band. Holes can be introduced either by the substitution of a divalent species (e.g., Mg^{2+} and Ca^{2+}) onto the octahedral trivalent *M*-cation site, or by the introduction of excess oxygen, in which case oxygen impurity bands may form.[13] We usually refer to the former process as "doping" or "Mg doping," and to the latter process as "intercalation" or "oxidation." Excess oxygen is located in, or very close to, the planes defined by the triangular arrangement of Cu atoms and in the centers of triangles (see Fig. 1). Further details regarding oxygen substitution can be found in an earlier publication.[14]

There has been no systematic study of the relative effectiveness of the different types of hole dopants (oxygen vs divalent cation), but it is an interesting question. $CuMO_2$ with *M* smaller than Sc does not admit excess O, so controllable hole doping for such delafossites can be achieved only by manipulation of the trivalent cation site (and in $CuAlO_2$ and $CuGaO_2$ even this has proven difficult). If *M* is larger than Sc, oxygen intercalation occurs and becomes increasingly likely for materials with the largest *M* cations, but the Cu–Cu distance increases with increasing size of the *M* cation, which tends to decrease the conductivity. $CuScO_2$ is a good intermediate case in which to test the efficacy of each type of dopant. Hole conduction in $CuMO_2$ appears to be predominantly in the Cu planes (the conductivity is anisotropic,[12] and the Cu-3*d* orbitals are the primary contributors to the top of the valence band). Excess oxygen is located in or near the Cu planes,[14] and increases the Cu–Cu distance, thus decreasing the overlap of Cu orbitals and tending to decrease conductivity, but the Cu–O bonds formed may increase the conductivity by providing a direct path. In

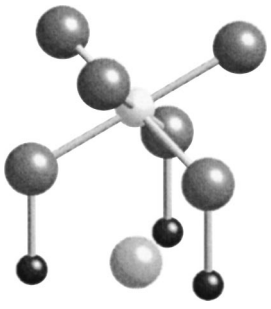

FIG. 1. Part of the AMO_2 delafossite structure showing the site of the O dopant. Small dark spheres are Cu atoms forming a triangle around the interstitial oxygen atom. The light sphere is a Sc atom (for which Mg substitutes) bonded to six oxygen atoms. In the 3R form, the interstitial oxygen atom is displaced by about 0.3 Å out of the Cu plane toward the Sc atom.[14]

principle, each excess O provides two holes, but it is not known if they are equally mobile, and it is even possible that one is completely localized. When Mg substitutes on the *M* cation site, much further from the planes, it is the source of a single hole. Since the *M* cation orbitals do not contribute to the band structure near the Fermi level, the Cu–O–M–O–Cu linkages are not major contributors to the hole conduction, and any hole produced by Mg substitution at *M* presumably migrates immediately to the Cu planes.

There are no reports of the effect of cation doping or O intercalation on the transport properties of bulk $CuSc_{1-x}Mg_xO_2$. In previous experiments on $CuSc_{1-x}Mg_xO_2$, the films had fixed Mg stoichiometry, and only changes induced by excess O were reported.[15] In the present study, both Mg and O were systematically changed in $CuScO_2$ powders and in films. This proved easier in the bulk form of the material, since Mg depletion occurred in the films, as described below. It is recognized that conductivity measurements on sintered powders necessarily reflect a lower bound on conductivity, and that processing effects on grain boundaries are very important. We were careful to keep processing conditions as consistent as possible.

II. EXPERIMENTAL DETAILS

Pressed pellets of $CuSc_{1-x}Mg_xO_2$ with $0.01<x<0.15$ were prepared from stoichiometric mixtures of CuO (Cerac, 99%), Sc_2O_3 (Stanford Materials, 99.95%), and MgO (Aldrich, 99%). The 12 mm diameter pellets were pressed at 4.5 tonnes producing material with 75%–85% of theoretical density. They were placed in a preheated oven, and held in air at 1100 °C for 20 h, after which they were quenched to room temperature. Mg doping of $CuScO_2$ stabilizes the hexagonal (2H) polymorph of the material, and all the x-ray diffraction patterns could be indexed to this polymorph alone. In addition, pure ($x=0$) $CuScO_2$ pellets were prepared, in both the 2H and 3R (rhombohedral) forms. To obtain phase pure 3R $CuScO_2$, a small (about 1%) Sc excess was used, and the pellet was heated in air at 600 °C/*h* to 1100 °C, held for 24 h and quenched. The phase pure 2H form was obtained by the same process as the Mg-doped samples, except that no MgO was used, but rather a small Cu excess.

Oxygen intercalation of pure 2H and 3R $CuScO_2$ and of Mg-doped $CuSc_{1-x}Mg_xO_2$ was achieved under 9×10^4 torr of oxygen at 420 °C for 6 days in a quartz tube. The intercalation was prohibitively slow in sintered material, but possible in powder or cold-pressed material, so the sintered pellets were reground, cold-pressed into bar form, and oxygen treated.

Films were prepared by rf sputtering from targets of $CuScO_2$, $CuSc_{0.95}Mg_{0.05}O_2$, and $CuSc_{0.85}Mg_{0.15}O_2$ in an Ar/O_2 (100:1.5) mixture at 12 mtorr. The substrate was pure amorphous SiO_2, held at temperatures between 150 °C and 350 °C. The deposition rate was about 0.02 nm/s and films were typically 150 nm thick. Following deposition, the brownish-tinted films were subjected to a 15 min rapid thermal anneal (RTA) cycle first in oxygen at 750 °C and then in argon at 900 °C. This process produces transparent, polycrystalline $CuSc_{1-x}Mg_xO_2$ films with only the slightest hint of color. Electron probe microanalysis revealed that the Mg content of the target was reproduced in the as-deposited films, but only approximately one-third of the Mg remained after the RTA process. Presumably the maximum Mg incorporated in films was 5% (i.e., $CuSc_{0.95}Mg_{0.05}O_2$) from the target with 15% Mg, but the fate of the rest of the Mg was not established. For consistency, films are referred to by the Mg content of the target from which they were prepared. Oxygen was intercalated by placing the films in a quartz tube furnace in 400 torr of O_2 at 400 °C for 9 h. In some cases, a high pressure intercalation process was conducted in a stainless steel tube furnace at 5×10^4 torr and 400 °C for 24 h.

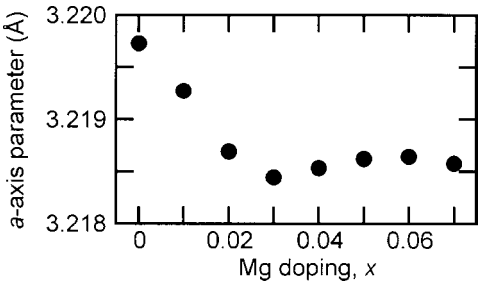

FIG. 2. Variation of the *a*-axis lattice parameter of $CuSc_{1-x}Mg_xO_2$ powders as a function of Mg doping.

In what follows, measurements are reported for samples with the same Mg content but different oxygen content. In the case of bulk material, two sintered pellets were produced under identical conditions from the same starting powder, ensuring identical Mg content, and one of the pellets was reground, cold pressed, and oxidized. In the case of films, a single sputtered film was cleaved into two smaller films that underwent identical treatment until the intercalation step.

The structure of the bulk material was examined by x-ray powder diffraction on a Siemens D5000 diffractometer with Cu $K\alpha$ radiation. For determination of accurate cell dimensions (Fig. 2), the cell edges were refined by least squares using data collected over 25–150° 2θ with a KCl internal standard. The oxygen content was analyzed by thermogravimetric analysis (TGA). Film structure was determined using a Rigaku Rapid diffractometer with the incident beam at grazing incidence and a curved image plate detector. The increase in oxygen content of the films was qualitatively established by electron microprobe measurements, and the increase of the lattice parameter upon oxygen intercalation and the darkening of the films confirm that oxygen uptake occurs.

Temperature-dependent conductivity measurements of pellets and films were conducted in a liquid nitrogen cryostat in the 120–290 K temperature range. Silver contacts were used to minimize contact resistance and a 4-probe colinear geometry was used for the unoxidized circular pellets. Silver contacts and a 4-probe technique appropriate to bar geometry were used for the oxidized samples. Several circular pellets of unoxidized material were modified to bar shape and their conductivities remeasured in the new geometry. Conductivities were reproducible within about 10%. The carrier type was determined by measurements of the Seebeck coefficient

at room temperature. A temperature gradient of about 3 K was established across the sample, and the resulting thermoelectric voltage was measured.

Diffuse reflectance spectra of powdered samples between 250 nm and 900 nm were obtained using a Xe lamp and a grating double monochromator as the source, and collecting light diffusely reflected by the powders with an integrating sphere and detecting it with a Si diode detector. These data were normalized to the signal obtained from MgO powder under the same conditions. The same source was used to measure reflection and transmission of the thin-film samples. In this case, no integrating sphere was necessary, since diffuse scattering is small.

III. RESULTS AND DISCUSSION

A. Structural properties

The $CuSc_{1-x}Mg_xO_2$ pellets (prior to oxygen intercalation) exhibited powder x-ray diffraction patterns that could be completely indexed to the 3R or 2H polymorphs of $CuScO_2$.[16] The diffraction patterns showed no evidence of second phase up to 5% Mg doping; at larger concentrations, small amounts of MgO and Cu_2O were present. The Mg doping results in a decrease of the *a* lattice parameter in powders up to 3% Mg doping as shown in Fig. 2. This indicates that Mg is incorporated in the $CuScO_2$ lattice up to a doping level of at least 3%. This is consistent with the Seebeck coefficient data presented in Fig. 6, although the conductivity data and x-ray diffraction refinement suggest a slightly higher ($\approx$5%) solubility. The substitution site for the Mg is the Sc site. The Mg^{2+} ionic radius (0.72 Å) is about 3% smaller than that of Sc^{3+} in the same coordination (0.745 Å),[17] which explains the lattice contraction upon substitution. Refinements of x-ray diffraction patterns of Mg doped $CuScO_2$ also support the site assignment. The 3R polymorph was obtained when no Mg was incorporated and a slight Sc excess was present. The 2H polymorph resulted for the Mg-doped samples and for the sample containing no Mg and a slight Cu excess, provided the powder was prepared in a preheated oven (slow heating always results in some 3R phase). The structural similarities between the Mg-doped material and the "Cu-doped" material suggest that the Cu excess necessary to stabilize the 2H form of $CuScO_2$ enters as Cu^{2+} on the Sc^{3+} site. The Cu^{2+} ion (0.73 Å) is an even closer match to the Sc^{3+} ion size, so this substitution is highly likely. Moreover, substitution of Cu^{2+} on an octahedral site is known to occur in the delafossite structure, for example, in $Cu_2(CuTi)O_4$.[18]

After oxidation of the pellets, the x-ray diffraction pattern exhibits interesting structure as shown in Fig. 3, where the pattern of intercalated 2H $CuSc_{0.95}Mg_{0.05}O_{2+y}$ is shown together with the pattern for unoxidized 2H $CuSc_{0.95}Mg_{0.05}O_2$. It is evident that each peak splits into two, and that one of the members of the split pair is closely aligned with the corresponding reflection in the unintercalated sample, while the other is shifted to smaller 2θ. The change is most striking for the (110) reflection near $2\theta = 57.3°$, with a shift of 0.8°. It is much smaller for the (00*l*) reflections,[14] and in this particular set, the data for the oxidized material include a small offset of 0.15° to bring the (004) reflections near $2\theta = 31.6°$ into alignment. The powder x-ray diffraction patterns indicate that the oxygenated powder is really an intimate mixture of two distinct compositions. More detailed studies[14] have shown that these compositions are very close to $CuScO_2$ and $CuScO_{2.5}$. (Note that here, $CuScO_{2.5}$ is the delafossite structure, which is either hexagonal or rhombohedral, with excess O in the Cu planes, and not $Cu_2Sc_2O_5$ which is orthorhombic and belongs to a different space group.) The extra oxygen entering the 2H lattice takes up interstitial sites in or close to the Cu plane and expands the *a* lattice parameter by about 1.5%. TGA of such samples revealed an average oxygen content between 2 and 2.5 per formula unit, as expected.

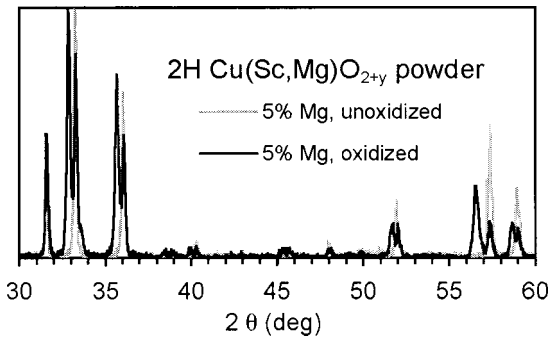

FIG. 3. X-ray diffraction patterns of unoxidized (light line) $CuSc_{0.95}Mg_{0.05}O_2$ and oxidized (dark line) $CuSc_{0.95}Mg_{0.05}O_{2+y}$ bulk powders. Two features are prominent: the splitting of the peaks in the oxygen-intercalated sample and the shift of one of the split pair to smaller 2θ. The shift is largest for (*hk*0) reflections.

Examples of the x-ray diffraction patterns of $CuSc_{0.99}Mg_{0.01}O_{2+y}$ films with $y \approx 0$ and $y \approx 0.5$ are presented in Fig. 4. The large shift of the (110) reflection is again evident, showing the increase in the *a* lattice parameter, and a very small effect on the (00*l*) reflections, and hence on the *c* axis parameter. The film reflections index to the 3R reflections, but some 2H component is present. The (*hk*0) and (00*l*) reflections are almost exactly coincident for 3R and 2H, and are therefore insensitive to stacking faults, which is why they are the narrowest and most symmetric peaks. Details of the thermal processing affect the formation of the different polytypes, and we are unable to control this well enough in films to produce a phase-pure polytype. There

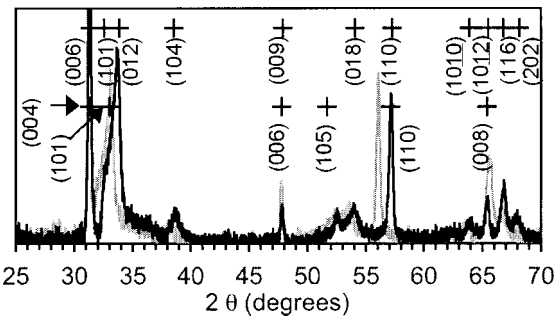

FIG. 4. X-ray diffraction patterns of unoxidized $CuSc_{0.99}Mg_{0.01}O_2$ (light line) and oxidized $CuSc_{0.99}Mg_{0.01}O_{2.5}$ (dark line) films. The important reflections of the 3R (above) and 2H (below) polytypes are indicated by crosses.

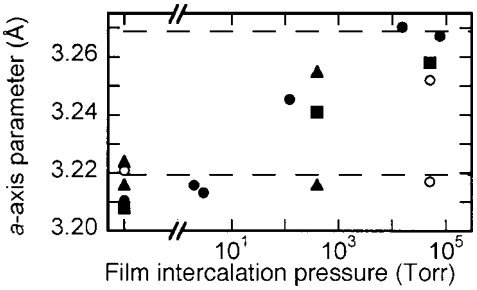

FIG. 5. Variation of the *a*-axis lattice parameter of $CuSc_{1-x}Mg_xO_{2+y}$ sputtered (closed symbols) and PLD (open symbols) films intercalated at 400 °C for ≈9 h as a function of intercalation pressure. Dashed lines indicate the *a*-axis parameters for bulk $CuScO_{2+y}$ for $y=0$ (below) and $y=0.5$ (above). Films that were not intercalated at all are plotted to the left of the break in the pressure axis.

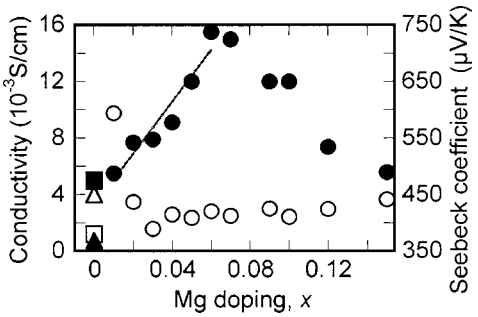

FIG. 6. Room temperature conductivity (closed symbols, left scale) and Seebeck coefficient (open symbols, right scale) of unoxidized $CuSc_{1-x}Mg_xO_2$ pellets. Circles correspond to Mg-doped material, squares to 2H $CuScO_2$, and triangles to 3R $CuScO_2$. The line is a fit to the conductivity data for $0.01<x<0.06$.

is a recent report of 3R epitaxial films of $CuScO_2$ deposited by pulsed laser deposition (PLD) on crystalline Al_2O_3.[5] Although the oxygen content could not be directly determined in our films, the value of the *a* axis lattice parameter is a good indicator. We usually determined this from the position of the (110) reflection, but a refinement of the spectrum was performed for several films, and the agreement is good. The powder data, extensively refined, give reference points for $y=0$ and $y=0.5$. In many films, we also observe the simultaneous presence of an unoxidized phase ($y\approx 0$) with an oxidized phase. In films, the *a* axis lattice parameter of the oxidized phase is consistent with values *other* than $y=0.5$, unlike in powders where only $y=0.5$ is observed for the oxidized portion. This difference is attributed to nonequilibrium conditions in the films, probably strain and other defects. Figure 5 shows the measured *a* lattice parameter for films as a function of oxygen intercalation pressure. The different symbols indicate different sets of films, which differ in Mg content, but, as noted previously, Mg incorporation has a negligible effect on the *a* axis lattice parameter. The films intercalated at 400 torr (solid triangle) and at 50 000 torr (open circle) are examples where two phases, one unoxidized and the other oxidized or partially oxidized, were identified by a clear splitting of the (110) reflection. It is worth noting that films made by pulsed laser deposition (open circle) were significantly more difficult to oxidize. These films were *c*-axis oriented in contrast to the polycrystalline sputtered films, and the slow oxidation characteristic of the bulk is also displayed here.

One other structural point is worth mentioning. Our procedure involves an oxidation step that results in the orthorhombic $Cu_2Sc_2O_5$ phase.[19] These films are polycrystalline and have a greenish hue. The subsequent reduction in Ar produces $CuScO_2$, which is almost colorless, but sometimes has a slight pink hue. There is no intrinsic reason why the production of $CuScO_2$ should proceed via the $Cu_2Sc_2O_5$ phase, and indeed we have produced films of $CuScO_2$ without this step, but it seems to be more reliable and reproducible to first oxidize the copper completely.[20]

B. Transport properties

The room temperature conductivity as a function of Mg doping for the unoxidized $CuSc_{1-x}Mg_xO_2$ pellets is shown in Fig. 6, along with the Seebeck coefficient for the same samples. There is an approximately linear increase in conductivity with increasing Mg content up to around $x=0.06$, where it reaches 1.5×10^{-2} S/cm. Further increase in the Mg content decreases the conductivity. Note that the conductivity of the "undoped" 2H $CuScO_2$ is comparable to the Mg-doped samples for small values of *x*. This supports the conjecture that the excess Cu necessary to stabilize the 2H phase enters as Cu^{2+} on the Sc^{3+} site and contributes a hole. The conductivities are more than an order of magnitude higher than for the 3R phase of $CuScO_2$. If one assumes that the conductivity can be written $\sigma=pe\mu$, where *p* is the number density of holes introduced by the Mg substitution and *e* the magnitude of the electronic charge, the data below $x=0.06$ can be reasonably well represented by a "mobility parameter" $\mu=5.8\times10^{-5}$ cm^2/V s. This is *not* a true mobility but a parameter that incorporates ionization efficiency as well as intrinsic mobility, but the low value is certainly consistent with the difficulty in measuring a Hall mobility in either powders or films, and indicates that the doping efficiency and the mobility are probably both small.

The Seebeck coefficients of all the samples are positive, indicating *p*-type conductivity. The values (400–500 μV/K) are typical of poor conductors, but more important is that the trends in the Seebeck coefficient mirror the conductivity measurement trends, with higher values for the less conductive samples and lower for more conductive ones. Since the Seebeck effect is less dependent on grain structure or sample geometry than conductivity, this indicates that the conductivity is probably not determined entirely by grain structure but rather reflects the Mg content. This is further supported by thin-film results where the conductivity of $CuSc_{1-x}Mg_xO_2$ is about the same order of magnitude as for powders in the same *x* range. Temperature-dependent conductivity measurements were also performed and reflect predominantly variable range hopping (VRH) character. VRH behavior follows the law

$$\sigma=\sigma_\infty e^{-(T_0/T)^{1/4}},$$

and can be characterized by the temperature parameter T_0, the slope of the graph of $\ln\sigma$ versus $T^{1/4}$. This parameter is presented in Table I, along with the sample densities.

TABLE I. Density (% of theoretical) and VRH parameter T_0 ($160 < T < 290$ K) from temperature-dependent conductivity measurements of unoxidized $CuSc_{1-x}Mg_xO_2$ pellets. In the case of undoped 2H $CuScO_2$, the phase was stabilized by a small Cu excess.

Mg doping x	Density (%)	$T_0^{1/4}$ ($K^{1/4}$)
0.0 (3R)	88	216
0.0 (2H)	77	168
0.01	76	180
0.02	76	167
0.03	80	160
0.04	83	163
0.05	83	163
0.06	81	162
0.07	85	154
0.09	85	154
0.10	83	154
0.12	85	139
0.15	83	150

We now turn to the results for the set of oxidized (intercalated) $CuSc_{1-x}Mg_xO_{2+y}$ pellets. The room temperature conductivities and Seebeck coefficients as a function of Mg content x are displayed in Fig. 7. The overall behavior is superficially similar to the unoxidized samples with a broad maximum near $x \approx 0.05$, but the conductivities are larger by about 1.5 orders of magnitude over those of the corresponding unoxidized pellets, with a maximum value of about 0.5 S/cm. Once again the Seebeck coefficient trend mirrors the conductivity trend, and the overall values are smaller by about a factor of 3–4, as expected for more conductive material. The increased conductivity is, of course, induced by the oxygen excess, which was measured by TGA for each sample, and Fig. 8 illustrates that the conductivity correlates with the oxygen excess. Figure 9 displays the conductivity, corrected by subtracting the small value for the corresponding unoxidized material, as a function of oxygen excess y. Again assuming the validity of $\sigma = pe\mu$, we calculate the number density on the premise of two holes per oxygen, and find that a "mobility parameter" of about 3.4×10^{-4} $cm^2/V\,s$ fits all the data reasonably well—there is also no saturation effect. As before, one should be circumspect about the interpretation of this parameter, but it is about a factor of 6 higher than the parameter found for the unoxidized materials. The difference in "mobility parameter" is significant but not extremely large. Thus the large conductivity of oxidized $CuSc_{1-x}Mg_xO_{2+y}$ can be mostly accounted for by the fact that $CuScO_2$ accommodates more excess oxygen than substituted Mg. Excess oxygen can be intercalated up to 0.5 f.u.$^{-1}$ (1 hole f.u.$^{-1}$ if both holes contribute to the conductivity), whereas Mg can be substituted only at the level of about 0.05 holes f.u.$^{-1}$ before adversely affecting conductivity.

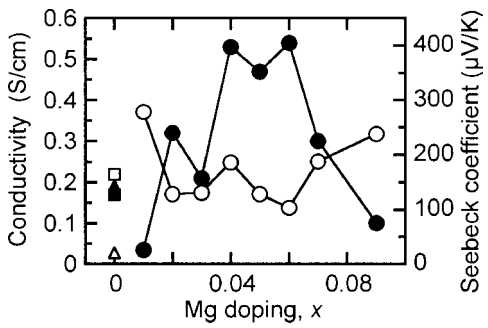

FIG. 7. Room temperature conductivity (closed symbols, left scale) and Seebeck coefficient (open symbols, right scale) of oxidized $CuSc_{1-x}Mg_xO_{2+y}$ pellets. Circles correspond to Mg-doped material, squares to 2H $CuScO_{2+y}$, and triangles to 3R $CuScO_{2+y}$.

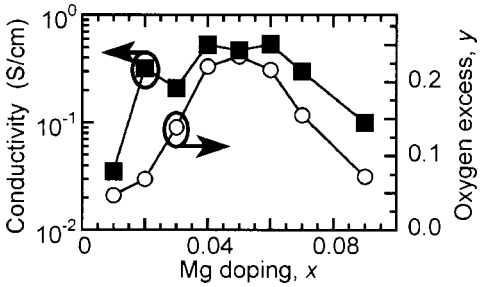

FIG. 8. Room temperature conductivity (closed symbols, left scale) and oxygen content as determined by TGA (open symbols, right scale) of oxidized $CuSc_{1-x}Mg_xO_{2+y}$ pellets as a function of Mg dopant concentration.

The oxygen excess represented in Fig. 9 is an average value for each sample—we have noted previously that the $CuSc_{1-x}Mg_xO_{2+y}$ powders are mixtures of phases with compositions close to $CuSc_{1-x}Mg_xO_2$ and $CuSc_{1-x}Mg_xO_{2.5}$. The intercalation of oxygen is very slow, so it is likely that each grain consists of an oxidized shell surrounding an unoxidized center.

It is not entirely clear why the oxygen uptake depends on the Mg doping at all, and why it peaks near the Mg solubility limit. Mg doping slightly *decreases* the $CuScO_2$ lattice parameter (see Fig. 2), so increased Mg content should inhibit oxygen uptake, not enhance it. It is in principle possible that the crystallite sizes were different for different Mg content, and this influenced the oxygen uptake. In favor of this argument is that all Mg doped materials were identified as the 2H polymorph, and this phase routinely has larger crystallite sizes and is more difficult to oxidize. Thus small variations in size could produce significant variations in average oxygen uptake. On the other hand, x-ray spectra provide no evidence for significant crystallite size variation. Whatever the reason for the observed larger oxygen uptake near $x \approx 0.5$, it raises an important question: could the "unoxidized" materials with similar x value have taken up a small amount of

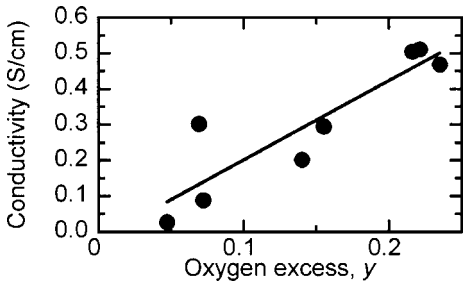

FIG. 9. Room temperature conductivity of oxidized $CuSc_{1-x}Mg_xO_{2+y}$ pellets as a function of average excess oxygen content. The conductivity of each corresponding unoxidized sample has been subtracted. The straight line is a fit.

TABLE II. Density (% of theoretical) and VRH parameter T_0 ($T<160$ K) from temperature-dependent conductivity measurements of oxidized $CuSc_{1-x}Mg_xO_{2+y}$ pellets. In the case of undoped 2H $CuScO_2$, the phase was stabilized by a small Cu excess.

Mg doping x	Density (%)	$T_0^{1/4}$ ($K^{1/4}$)
0.0 (3R)	67	111
0.0 (2H)	80	79
0.01	75	57
0.02	76	56
0.03	71	68
0.04	75	68
0.05	71	77
0.06	79	71
0.07	73	67
0.09	79	64

oxygen during synthesis (for example, during the quench from 1100 °C), so that their conductivity is really oxygen induced rather than Mg induced? The answer appears to be "no" for several reasons. First, neither TGA nor x-ray diffraction of the unoxidized $CuSc_{1-x}Mg_xO_2$ materials gives any indication of excess oxygen. Second, the oxidized materials were ground one additional time compared to their unoxidized counterparts, so crystallite size variations should be different. Finally, thin film conductivity results, discussed below, also show that the addition of Mg improves conductivity.

The oxidized 3R and 2H phases of bulk $CuScO_{2+y}$ (no Mg) also show changes in transport properties similar to their unoxidized counterparts. The oxidized 2H $CuScO_{2+y}$ (Cu doped) is of comparable conductivity to the oxidized Mg-doped powders. In the case of the 3R $CuScO_{2+y}$, the improvement in conductivity upon oxidation is very large (from 7×10^{-4} S/cm to 0.2 S/cm upon oxidation). This may result from increased oxygen incorporation arising from the generally smaller grain sizes in 3R powder.[14] The conductivity of all the oxidized materials is less temperature dependent than for the corresponding unoxidized materials, which results in lower values of the parameter T_0, as shown in Table II. It is also not possible to fit all the data with a single VRH form, so the values in Table II are for temperatures below 160 K.

The conductivity for $CuSc_{1-x}Mg_xO_{2+y}$ films as a function of Mg content in the sputter target is shown in Fig. 10. Unoxidized films with no Mg doping ($y=0, x=0$) have very low conductivities ($<10^{-4}$ S/cm), and the incorporation of Mg increases the conductivity by about two orders of magnitude to the level of 10^{-2} S/cm (similar to powders). The conductivity of the film with higher Mg content ($x=0.15$ in sputter target) is slightly smaller than that of the film with $x=0.05$ in the sputter target. Although there are only two doping levels, the results are consistent for several preparation conditions (including more than the two shown here). The overall increase of the conductivity upon uptake of oxygen is a further two orders of magnitude to a level of 1–5 S/cm for the films intercalated at 400 torr. In this case the conductivity continues to increase with increasing Mg doping. Upon high pressure oxygen intercalation (5×10^4 torr), the conductivity reached about 25 S/cm for undoped and Mg doped films. We have no quantitative measure of the oxygen content of the films, but films intercalated with oxygen at 400 torr were all intercalated simultaneously, so the oxygen uptake should be the same. The increased conductivity for higher Mg doping in this case could be the result of a codoping effect where the presence of the oxygen improves the efficiency of hole generation by the Mg, or improves their mobility by providing increased orbital overlap in the Cu planes (or Cu–O planes in this case). However, this would have to be investigated more carefully for several levels of Mg doping, and would require quantitative oxygen analysis. In the heavily intercalated films, the conductivity is high enough that the dependence on Mg concentration is no longer evident. The maximum conductivity achieved in intercalated films is 10–50 times higher than in powders. Since the conductivity for the unoxidized films and powders is similar, the lower conductivity in powders is unlikely to be due to grain boundary effects, but rather to incomplete oxidation of the powdered materials.

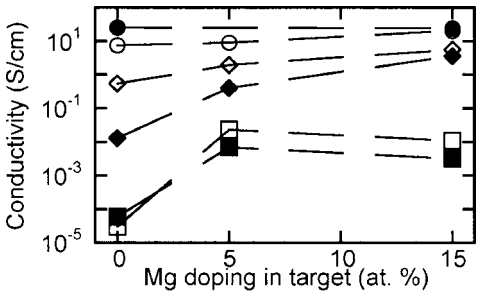

FIG. 10. Room temperature conductivity of $CuSc_{1-x}Mg_xO_{2+y}$ films. The Mg content is indicated as the percentage of Mg in the sputter target. Three different intercalation procedures—high pressure (circles), intermediate pressure (diamonds), and no intercalation (squares)—and two different deposition temperatures of 350 °C (closed symbols) and 150 °C (open symbols) are also indicated. The lines are guides to the eye.

C. Optical properties

The results of the diffuse reflectance measurements of the unoxidized 3R and 2H $CuScO_2$ powders and of unoxidized $CuSc_{1-x}Mg_xO_2$ powders for $x=0.02$ and 0.04 are graphed in Fig. 11. The diffuse reflectance (relative to MgO), $R(\lambda)$, was recorded as a function of wavelength. The ratio $(1-R)^2/2R$ gives the ratio of the absorption coefficient to the scattering factor at that particular wavelength. To the extent that scattering is not expected to vary considerably over the wavelength of interest, this ratio may be considered propor-

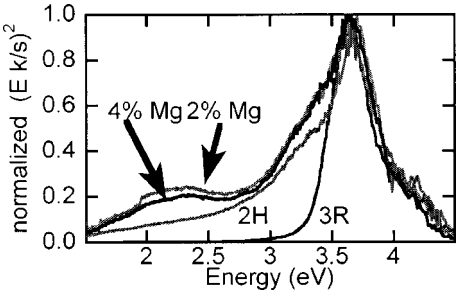

FIG. 11. Diffuse reflectance spectra of $CuSc_{1-x}Mg_xO_2$ powders.

tional to the absorption coefficient, usually called α. The absorption coefficient can be obtained directly from true transmission and reflection measurements on thin films or crystals, but for powders, diffuse reflection is considered a reasonable equivalent. (Diffusely "reflected" light from loose powders has, in fact, also been transmitted through tiny crystallites near the surface.) It is common practice to plot $(\alpha E)^2$ versus E (where $E=hc/\lambda$ is the photon energy) and determine a direct band gap from the intercept of the plot with the ordinate axis. Such a representation is found in Fig. 11. The values for the band gap thus determined from diffuse reflectance may not be entirely accurate given by the approximations, but they should clearly indicate trends.

The 3R $CuScO_2$ is very slightly gray in color and its diffuse reflectance spectrum is very clean and allows an unambiguous band gap to be identified. It was estimated at about 3.3 eV and is qualitatively in agreement with values measured in thin films.[15,5] The "undoped" 2H phase $CuScO_2$ powder is a darker gray as is to be expected from the overall higher absorption in the visible region. There is also an additional feature in diffuse reflectance near 3.3 eV. However, the spectrum looks very similar to that of the 3R material above about 3.4 eV, and it would be difficult to argue that the band gap has been decreased. Rather, it appears that the incorporation of excess Cu^{2+} introduces states in the gap that contribute to absorption. Incorporation of Mg^{2+} into the samples further darkens the material as is evidenced by increased absorption near 2.3 eV for both the $x=0.02$ and $x=0.04$ powders. The oxidation process converted all the $CuScO_2$ and $CuSc_{1-x}Mg_xO_2$ samples to black powders that were too absorbent to produce meaningful diffuse reflectance spectra.

Reflection and transmission spectra of films confirm the visual impression that $CuScO_2$ films are transparent in the visible region, and are not rendered more absorbing by the incorporation of Mg at the levels investigated here. These films have a direct band gap of 3.6 eV. Intercalation of oxygen causes increased absorption across the visible spectrum. The highly conductive films darken, but retain transmission around 70% for wavelengths longer than 700 nm. At 550 nm, transmission is about 50%, and decreases for shorter wavelengths.

IV. SUMMARY

Changes in structural and transport properties of $CuScO_2$ powders and films upon substitution of Mg for Sc and intercalation of oxygen are reported. Mg doping and oxygen intercalation both increase *p*-type conductivity in $CuScO_2$, and the conductivity can be varied by five orders of magnitude with various combinations of dopants. The effectiveness of each type doping appears to be similar, and the larger conductivity resulting from oxygen intercalation is most simply explained by the capacity of the structure to incorporate a large oxygen excess (up to $y=0.5$ in $CuSc_{1-x}Mg_xO_{2+y}$) with continued increase in conductivity, whereas its ability to substitute Mg is limited to $x<0.06$.

Oxygen intercalation expands the $CuScO_2$ lattice, mainly by increasing the *a* axis lattice parameter. X-ray diffraction indicates that the oxidized bulk material consists of a mixture of two phases with compositions close to $CuSc_{1-x}Mg_xO_{2.0}$ and $CuSc_{1-x}Mg_xO_{2.5}$. In films, such mixtures are also observed, but the oxygen content of the oxidized phase may be less than 2.5.

The increased conductivity $CuSc_{1-x}Mg_xO_{2+y}$ has a significant effect on the optical absorption of the material. Diffuse reflectivity of powders indicates that the 3R polymorph is virtually defect free, with little absorption of light at energies below 3.4 eV. The 2H polymorph stabilized by excess Cu shows increased absorption across the visible spectrum, as do the 2H polymorphs stabilized by Mg substitution, which also have additional absorption at 2.3 eV. Films of $CuSc_{1-x}Mg_xO_2$ are highly transparent, even with Mg substituted at the level of several percent, but show increased absorption over the visible range upon oxygen intercalation.

ACKNOWLEDGMENTS

We thank A. Draeseke for early contributions to the thin film preparation, Dr. R. Nagarajan for preliminary x-ray data analysis, Professor W. W. Warren for numerous useful discussions, and Dr. A. Yokochi for x-ray diffraction of thin films. This work was partially supported by the National Science Foundation Grant No. (DMR 0071727 and DMR 0245386), by the Army Research Office Grant No. (E-18-667-G3), and by the Research Corporation.

[1] J. Li, A. Yokochi, T. G. Amos, and A. W. Sleight, Chem. Mater. **14**, 2602 (2002).
[2] R. J. Cava, W. F. Peck, Jr., J. J. Krajewski, S-W. Cheong, and H. Y. Hwang, J. Mater. Res. **9**, 314 (1994).
[3] K. Isawa, Y. Yaegashi, S. Ogota, M. Nagano, S. Sudo, K. Yamada, and H. Yamauchi, Phys. Rev. B **57**, 7950 (1998).
[4] N. Duan, A. W. Sleight, M. K. Jayaraj, and J. Tate, Appl. Phys. Lett. **77**, 1325 (2000).
[5] Y. Kakehi, S. Nakao, K. Satoh, and T. Yotsuya, Thin Solid Films **445**, 294 (2003).
[6] H. Yanagi, S. Inoue, K. Ueda, H. Kawazoe, H. Hosono, and N. Hamada, J. Appl. Phys. **88**, 4159 (2000).
[7] H. Yanagi, T. Hase, S. Ibuki, K. Ueda, and H. Hosono, Appl. Phys. Lett. **78**, 1583 (2001).
[8] K. Ueda, T. Hase, H. Yanagi, H. Kawazoe, H. Hosono, H. Ohta, M. Orita, and M. Hirano, J. Appl. Phys. **89**, 1790 (2001).
[9] R. J. Cava, H. W. Zandbergen, A. P. Ramirez *et al.*, J. Solid State Chem. **104**, 437 (1993).
[10] F. A. Benko and F. P. Koffyberg, Can. J. Phys. **63**, 1306 (1985).
[11] F. A. Benko and F. P. Koffyberg, Phys. Status Solidi A **94**, 231 (1986).
[12] D. B. Rogers, R. D. Shannon, C. T. Prewitt, and J. L. Gilson, Inorg. Chem. **10**, 723 (1971).
[13] L. F. Mattheiss, Phys. Rev. B **R48**, 18300 (1993).
[14] J. Li, A. F. T. Yokochi, and A. W. Sleight, Solid State Sci. **6**, 831 (2004).
[15] H. Yanagi, S. Park, A. D. Draeseke, D. A. Keszler, and J. Tate, J. Solid State Chem. **175**, 34 (2003).
[16] International Center for Diffraction Data, JCPDS 79-0599, 77-2496.
[17] Effective ionic radii from R. D. Shannon, Acta Crystallogr., Sect. A: Found. Crystallogr. **32**, 751, (1976).
[18] K. Hayashi and M. Kato, Nihon Kagaku Kaishi **1**, 6 (1974)
[19] International Center for Diffraction Data, JCPDS 83-1256.
[20] B. Nielsen, M.S. Thesis, Oregon State University, 2004 (unpublished).